

Simulating the charged charmoniumlike structure $Z_c(4025)$

Xiao Wang^{1,2}, Yuan Sun^{1,2}, Dian-Yong Chen^{1,3,a}, Xiang Liu^{1,2,b}, Takayuki Matsuki^{4,c}

¹ Research Center for Hadron and CSR Physics, Lanzhou University and Institute of Modern Physics of CAS, Lanzhou 730000, China

² School of Physical Science and Technology, Lanzhou University, Lanzhou 730000, China

³ Nuclear Theory Group, Institute of Modern Physics, Chinese Academy of Sciences, Lanzhou 730000, China

⁴ Tokyo Kasei University, 1-18-1 Kaga, Itabashi, Tokyo 173-8602, Japan

Received: 18 November 2013 / Accepted: 29 January 2014 / Published online: 19 February 2014

© The Author(s) 2014. This article is published with open access at Springerlink.com

Abstract Inspired by the recent observation of the charged charmoniumlike structure $Z_c(4025)$, we explore the $Y(4260) \rightarrow (D^*\bar{D}^*)\pi^+$ decay through the initial-single-pion-emission mechanism, where the $D^*\bar{D}^* \rightarrow D^*\bar{D}^*$ interaction is studied by the ladder approximation, including the non-interacting case. Our calculation of the differential decay width for $Y(4260) \rightarrow (D^*\bar{D}^*)\pi^+$ indicates that a charged enhancement structure around $D^*\bar{D}^*$ appears in the $D^*\bar{D}^*$ invariant mass spectrum for this process, which might correspond to the newly observed $Z_c(4025)$ structure.

1 Introduction

Very recently, the BESIII Collaboration announced the observation of a charged charmoniumlike structure, $Z_c(4025)$, which appears in the π^\mp recoil mass spectrum of $e^+e^- \rightarrow (D^*\bar{D}^*)^\pm\pi^\mp$ at $\sqrt{s} = 4.26$ GeV. Its mass and width are $M = (4026.3 \pm 2.6 \pm 3.7)$ MeV and $\Gamma = (24.8 \pm 5.6 \pm 7.7)$ MeV [1]. Thus, $Z_c(4025)$ is near the $(D^*\bar{D}^*)^\pm$ threshold.

Before the observation of $Z_c(4025)$, the Belle Collaboration reported a charged bottomoniumlike structure $Z_b(10650)$ by studying $\Upsilon(10860) \rightarrow (B^*\bar{B}^*)^\pm\pi^\mp$ [2], where $Z_b(10650)$ is near the $(B^*\bar{B}^*)^\pm$ threshold. The similarity between $Z_c(4025)$ and $Z_b(10650)$ indicates that $Z_c(4025)$ can be seen as the counterpart of $Z_b(10650)$. In Ref. [3], we have proposed an explanation in terms of the initial-single-pion-emission (ISPE) mechanism proposing the reason why $Z_b(10650)$ exists in the decay $\Upsilon(10860) \rightarrow (B^*\bar{B}^*)^\pm\pi^\mp$. What is more important is that we have already predicted a charged structure near the $D^*\bar{D}^*$ threshold in

the $(D^*\bar{D}^*)^\pm$ invariant mass spectrum of $\psi(4415) \rightarrow (D^*\bar{D}^*)^\pm\pi^\mp$ in the same paper.

This recent experimental discovery of $Z_c(4025)$ provides us with more opportunities to further reveal the underlying mechanism behind this novel phenomenon. In the past decades, the experimental search for exotic states beyond the conventional hadron configurations is an important and intriguing research topic. The peculiarities of $Z_c(4025)$ immediately lead us to recognize that $Z_c(4025)$ might be the most reliable candidate as an exotic state. However, before giving a one-sided view, we need to exhaust all the possibilities under the conventional frameworks.

In this manner, in this paper we analyze the decay process $Y(4260) \rightarrow (D^*\bar{D}^*)^\pm\pi^\mp$ via the ISPE mechanism or its extension to include higher orders. This mechanism [4] was first proposed to understand why two the bottomoniumlike structures $Z_b(10610)$ and $Z_b(10650)$ can be found in the $\Upsilon(nS)\pi^\pm$ ($n = 1, 2, 3$) and $h_b(mP)\pi^\pm$ ($m = 1, 2$) invariant mass spectra of $e^+e^- \rightarrow \Upsilon(nS)\pi^+\pi^-$, $h_b(mP)\pi^+\pi^-$ at $\sqrt{s} = 10865$ MeV [5]. Later, the ISPE mechanism had been extensively applied to the study of the hidden-charm dipion/dikaon decays of higher charmonia and charmoniumlike states [6–8], the hidden-bottom dipion decays of $\Upsilon(11020)$ [9], and the hidden-strange dipion decays of $Y(2175)$ [10], where many novel phenomena of the charged enhancement structures have been predicted. In this work, by studying the process $Y(4260) \rightarrow (D^*\bar{D}^*)\pi^+$, we expect to answer the question whether the newly observed charged structure $Z_c(4025)$ can be explained by the ISPE mechanism, which is an intriguing research topic, too, as regards the search for the underlying mechanism behind this kind of novel phenomena.

This work is organized as follows. After the introduction, we present the calculation of $Y(4260) \rightarrow (D^*\bar{D}^*)^\pm\pi^\mp$ via an extension of the ISPE mechanism, where the description of the interaction $D^{*0}D^{*-} \rightarrow D^{*0}D^{*-}$ is given by the ladder diagrams applying an effective Lagrangian approach.

^a e-mail: chendy@impcas.ac.cn

^b e-mail: xiangliu@lzu.edu.cn

^c e-mail: matsuki@tokyo-kasei.ac.jp

In Sect. 3, the numerical results are shown in comparison with the experimental data. The last section is a short summary.

2 $Y(4260) \rightarrow (D^* \bar{D}^*)^- \pi^+$ decay

The ISPE mechanism for $Y(4260) \rightarrow (D^* \bar{D}^*)^- \pi^+$ is shown by the diagram in Fig. 1. Due to this mechanism, the emitted pion from the $Y(4260)$ decay plays a very important role and has a continuous energy distribution, which easily enables D^{*0} and D^{*-} with low momenta to interact with each other. Thus, in the following our main task is to describe the $D^{*0} D^{*-} \rightarrow D^{*0} D^{*-}$ interaction and combine this reaction with the corresponding $Y(4260)$ decay. In this work, we include a tree diagram, i.e., the case that the kernel does not include an interaction.

To calculate the $D^{*0} D^{*-} \rightarrow D^{*0} D^{*-}$ interaction near the threshold as depicted by a gray kernel shown in Fig. 1, we adopt a ladder approximation as presented in Fig. 3, where we borrow some ideas from the Bethe–Salpeter equation [11]. After expanding the amplitude by a partial wave basis, the ladder diagrams with n loops can be expressed as a geometric series, which allows us to sum over all the ladder diagrams (see the first row in Fig. 3). This treatment is allowed when the higher loop contribution is as large as the lower-order one. In order to have a geometric series we make a further approximation for the ladder diagrams to insert cuts in between all the white kernels as shown in the first row of Fig. 1. Furthermore, in this work we introduce a pion exchange and a contact term as the main contributions to the direct $D^{*0} D^{*-} \rightarrow D^{*0} D^{*-}$ interaction as listed in the second row of Fig. 3 depicted by the white kernel which is included in the gray kernel. The contact term can be regarded as an effective one due to the collection of heavier particle exchanges other than the pion and hence there appears a relative phase to the one-pion exchange term. Here, we need to emphasize that we may use only a contact term to construct a much simpler model assuming that one-pion exchange can be approximated by a contact term. However, one-pion exchange actually denotes the long-distant contribution, while the contact term reflects the short-distant contribution from the heavier meson exchanges. Considering these facts, we would like to introduce both the one-pion exchange and the contact terms.

In the following, we first give the general formula describing the two body \rightarrow two body process.

Before obtaining a total amplitude of Fig. 1 and all the ladder diagrams of the first row of Fig. 3, we need to consider the following items and prescriptions.

1. Feynman diagrams in Fig. 3 are directly described in terms of two-particle bases, $|p_1, p_2, s_1, s_2, \sigma_1, \sigma_2\rangle$, in the initial and final states. On the other hand, a simple rela-

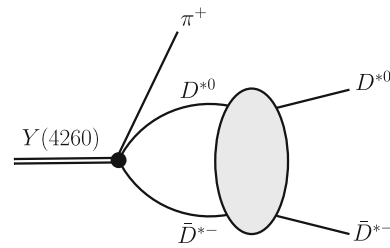


Fig. 1 The typical diagram depicting $Y(4260) \rightarrow \pi^+ D^{*0} D^{*-}$ via the ISPE mechanism. Here, the gray kernel represents the $D^{*0} D^{*-} \rightarrow D^{*0} D^{*-}$ interaction given in Fig. 3

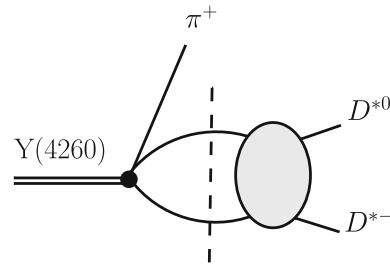


Fig. 2 The diagram in which a cut is inserted in Fig. 1 which is used to calculate the final total amplitude

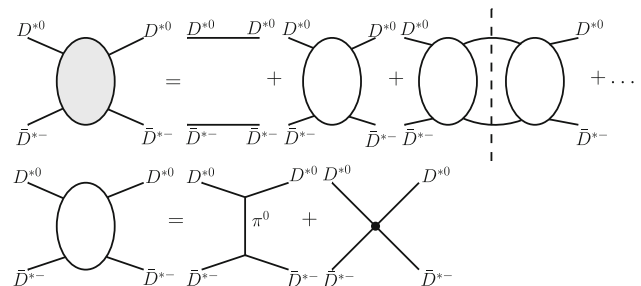


Fig. 3 The ladder approximation denoted by a gray blob for the $D^{*0} D^{*-} \rightarrow D^{*0} D^{*-}$ interaction. Here, we consider an elementary contribution of the four-point vertex coming from the pion exchange and the contact term denoted by a white blob. The vertical dashed line is a cut

tion between gray and white blobs is obtained if they are expressed in terms of a partial wave basis, $|p, j, \sigma, \ell, s\rangle$. Detailed properties of these bases which are used in deriving equations below are given in the appendix.

2. Insert cuts in all the places in a gray blob where two propagators connecting two white blobs like the first row in Fig. 3 appear.
3. Expand the gray blob in terms of the white blobs.
4. Attach the tree vertex, $Y(4260)\pi^+ D^{*0} D^{*-}$, to the gray blob in Fig. 3.
5. One cut is now inserted between the vertex and the gray blob, as in Fig. 2, so that the total amplitude in Fig. 1 can be seen as a multiplication of the tree vertex, $Y(4260)\pi^+ D^{*0} D^{*-}$, and the approximate ladder diagrams.

Using Eq. (20), the gray and white blobs are expressed as

$$\langle q, \tilde{j}, \tilde{\sigma}, \tilde{\ell}, \tilde{s} | T | p, j, \sigma, \ell, s \rangle = \mathcal{T}^{(j)}(p)_{\tilde{\ell}, \tilde{s}}^{\tilde{\ell}, \tilde{s}} \delta^4(p - q), \quad (1)$$

$$\langle q, \tilde{j}, \tilde{\sigma}, \tilde{\ell}, \tilde{s} | T_0 | p, j, \sigma, \ell, s \rangle = \mathcal{T}_0^{(j)}(p)_{\tilde{\ell}, \tilde{s}}^{\tilde{\ell}, \tilde{s}} \delta^4(p - q), \quad (2)$$

which are expressed in partial wave bases, and T and T_0 are the corresponding T matrices, respectively. Following items 2 and 3 above, the diagrams listed in the first row of Fig. 3 can be finally described by the series

$$\begin{aligned} \mathcal{T}^{(j)}(p) &= 1 + i\beta \mathcal{T}_0^{(j)}(p) + (i\beta)^2 \mathcal{T}_0^{(j)}(p) \mathcal{T}_0^{(j)}(p) + \cdots \\ &= \frac{1}{1 - i\beta \mathcal{T}_0^{(j)}(p)}, \end{aligned} \quad (3)$$

where $\beta = (2\pi)^4/2$, all the indices are suppressed, and we have the amplitude $\mathcal{T}_0^{(j)}(p)_{\tilde{\ell}, \tilde{s}}^{\tilde{\ell}, \tilde{s}}$, which consists of the one-pion exchange contribution and the contact term. All the quantities included in Eq. (3) should be tacitly understood to be matrices and should be accordingly multiplied with each other.

Thus, by inserting the completeness condition for the two-particle basis given by Eq. (15) we can express $\mathcal{T}_0^{(j)}(p)_{\tilde{\ell}, \tilde{s}}^{\tilde{\ell}, \tilde{s}}$ as

$$\begin{aligned} \mathcal{T}_0^{(j)}(p)_{\tilde{\ell}, \tilde{s}}^{\tilde{\ell}, \tilde{s}} \delta^4(p - q) \\ \equiv \langle q, \tilde{j}, \tilde{\sigma}, \tilde{\ell}, \tilde{s} | T_0 | p, j, \sigma, \ell, s \rangle \\ = \sum_{s'_1, s'_2, \sigma'_1, \sigma'_2} \int d^3 \tilde{p}_1 d^3 \tilde{p}_2 d^3 \tilde{p}'_1 d^3 \tilde{p}'_2 \\ \times \langle q, \tilde{j}, \tilde{\sigma}, \tilde{\ell}, \tilde{s} | \mathbf{p}_1, s_1, \sigma_1; \mathbf{p}_2, s_2, \sigma_2 \rangle \\ \times \langle \mathbf{p}'_1, s'_1, \sigma'_1; \mathbf{p}'_2, s'_2, \sigma'_2 | p, j, \sigma, \ell, s \rangle \\ \times \langle \mathbf{p}_1, s_1, \sigma_1; \mathbf{p}_2, s_2, \sigma_2 | T_0 | \mathbf{p}'_1, s'_1, \sigma'_1; \mathbf{p}'_2, s'_2, \sigma'_2 \rangle \end{aligned} \quad (4)$$

with $d^3 \tilde{p} = d^3 p / ((2\pi)^3 2E_p)$.

Having the above preparation and using the effective Lagrangian approach, we illustrate how to obtain the matrix element $\langle \mathbf{p}_1, s_1, \sigma_1; \mathbf{p}_2, s_2, \sigma_2 | T_0 | \mathbf{p}'_1, s'_1, \sigma'_1; \mathbf{p}'_2, s'_2, \sigma'_2 \rangle$ for the $D^{*0} D^{*-} \rightarrow D^{*0} D^{*-}$ interaction discussed. The effective Lagrangians involved are given by

$$\begin{aligned} \mathcal{L}_{Y(4260) D^{*} D^{*} \pi} &= -i g_{Y D^{*} D^{*} \pi} \epsilon^{\mu\nu\rho\sigma} Y_{\mu} D_{\nu}^{*} \partial_{\rho} \pi \bar{D}_{\sigma}^{*} \\ &\quad - i h_{Y D^{*} D^{*} \pi} \epsilon^{\mu\nu\rho\sigma} \partial_{\mu} Y_{\nu} D_{\rho}^{*} \pi \bar{D}_{\sigma}^{*}, \end{aligned} \quad (5)$$

$$\begin{aligned} \mathcal{L}_{D^{*} D^{*} D^{*} D^{*}} &= g_c \left(2 \bar{D}_{\nu}^{* \dagger} D_{\mu}^{*} \bar{D}^{* \dagger \nu} D^{* \mu} - \bar{D}_{\mu}^{* \dagger} D^{* \mu} \bar{D}_{\nu}^{* \dagger} D^{* \nu} \right. \\ &\quad \left. - \bar{D}_{\mu}^{* \dagger} D_{\nu}^{*} \bar{D}^{* \dagger \nu} D^{* \mu} \right), \end{aligned} \quad (6)$$

$$\mathcal{L}_{D^{*} D^{*} \pi} = -g_{D^{*} D^{*} \pi} \epsilon^{\mu\nu\rho\sigma} \partial_{\mu} D_{\nu}^{*} \pi \partial_{\rho} \bar{D}_{\sigma}^{*}, \quad (7)$$

where these Lorentz structures are given in Refs. [12–16]. These effective Lagrangians are obtained by assuming the $SU(2)$ invariance among couplings of the $SU(2)$ pseudoscalar and vector multiplets as usual. The coupling constant $g_{D^{*} D^{*} \pi}$ can be related to the $D^{*} \rightarrow D\pi$ decay [17]

and, hence, $g_{D^{*} D^{*} \pi} = 8.94 \text{ GeV}^{-1}$ is obtained [18]. However, the coupling constants $g_{Y D^{*} D^{*} \pi}$ and $h_{Y D^{*} D^{*} \pi}$ cannot be constrained since they are related to the inner structure of $Y(4260)$. In this work, we will discuss the line shapes of the $D^{*0} D^{*-}$ invariant mass spectra when taking different values of $\xi = h_{Y D^{*} D^{*} \pi} / g_{Y D^{*} D^{*} \pi}$.

The amplitude for the interaction $D^{*0}(p_2, \epsilon_2) D^{*-}(p_1, \epsilon_1) \rightarrow D^{*0}(p_4, \epsilon_4) D^{*-}(p_3, \epsilon_3)$ by exchanging one pion is

$$\begin{aligned} \mathcal{A}_{\pi\text{-exchange}} &= -g_{D^{*} D^{*} \pi}^2 \epsilon^{\mu\nu\rho\sigma} p_{1\mu} \epsilon_{1\nu} p_{3\rho} \epsilon_{3\sigma}^* \frac{1}{q^2 - m_{\pi}^2} \\ &\quad \times \epsilon^{\alpha\beta\gamma\delta} p_{4\alpha} \epsilon_{4\beta}^* p_{2\gamma} \epsilon_{2\delta}, \end{aligned} \quad (8)$$

while the amplitude for the contact term reads

$$\begin{aligned} \mathcal{A}_{\text{contact}} &= g_{D^{*} D^{*} D^{*} D^{*}}^2 [4(\epsilon_2 \cdot \epsilon_3^*)(\epsilon_1 \cdot \epsilon_4^*) - 2(\epsilon_2 \cdot \epsilon_4^*) \\ &\quad \times (\epsilon_1 \cdot \epsilon_3^*) - 2(\epsilon_1 \cdot \epsilon_2)(\epsilon_3^* \cdot \epsilon_4^*)]. \end{aligned} \quad (9)$$

In addition, the tree amplitude of the direct $Y(4260)(p, \epsilon_Y) \rightarrow D^{*0}(p_2, \epsilon_2) D^{*-}(p_1, \epsilon_1) \pi^+(k)$ decay is

$$\begin{aligned} \mathcal{A}_{Y D^{*} D^{*} \pi} &= -g_{Y D^{*} D^{*} \pi} \epsilon^{\mu\nu\rho\sigma} \epsilon_{1\mu}^* \epsilon_{2\nu}^* \epsilon_{Y\rho} \\ &\quad \times (5k + p_1 + p_2 + 3\xi p)_{\sigma}. \end{aligned} \quad (10)$$

As for the process $D^{*0} D^{*-} \rightarrow D^{*0} D^{*-}$, the matrix element $\langle \mathbf{p}_1, s_1, \sigma_1; \mathbf{p}_2, s_2, \sigma_2 | T_0 | \mathbf{p}'_1, s'_1, \sigma'_1; \mathbf{p}'_2, s'_2, \sigma'_2 \rangle$ in Eq. (4) can be further expressed as

$$\begin{aligned} \langle \mathbf{p}_1, s_1, \sigma_1; \mathbf{p}_2, s_2, \sigma_2 | T_0 | \mathbf{p}'_1, s'_1, \sigma'_1; \mathbf{p}'_2, s'_2, \sigma'_2 \rangle \\ = \mathcal{A}_{\pi\text{-exchange}} + e^{i\phi} \mathcal{A}_{\text{contact}}, \end{aligned} \quad (11)$$

where the phase ϕ is introduced.

Following item 3, we need to insert the cut in between the tree vertex and the gray blob as in Fig. 2. There have been a couple of examples to calculate the decay amplitudes by inserting a cut between a tree vertex and other diagrams. See, e.g., Refs. [19, 20] and [21]. Finally, by using Eq. (3), the total partial wave amplitude for the process $Y(4260) \rightarrow \pi^+ D^{*0} D^{*-}$ discussed in this work becomes

$$\mathcal{T}_{\text{total}}^{(j)}(p)_{\tilde{\ell}, \tilde{s}}^{\tilde{\ell}, \tilde{s}} = \mathcal{T}^{(j)}(p)_{\tilde{\ell}, \tilde{s}}^{\tilde{\ell}, \tilde{s}} \mathcal{T}_{Y D^{*} D^{*} \pi}^{(j)}(p)_{\tilde{\ell}, \tilde{s}}^{\ell', s'}, \quad (12)$$

where $\mathcal{T}_{Y D^{*} D^{*} \pi}^{(j)}(p)_{\tilde{\ell}, \tilde{s}}^{\ell', s'}$ is the tree amplitude given by Eq. (10) expressed in a partial wave basis like in Eq. (4).

Summing over all $\mathcal{T}_{\text{total}}^{(j)}(p)_{\tilde{\ell}, \tilde{s}}^{\tilde{\ell}, \tilde{s}}$ partial amplitudes with different quantum numbers, we get the total amplitude \mathcal{M} . The differential decay width reads

$$d\Gamma = \frac{1}{(2\pi)^5 16 M_{Y(4260)}^2} |\mathcal{M}|^2 |\mathbf{p}_{\pi}| d m_{D^{*} \bar{D}^{*}} d\Omega_{D^{*}} d\Omega_{\pi}, \quad (13)$$

where \mathbf{p}_{π} is the three-momentum of the emitted pion in the rest frame of $Y(4260)$, while $(\mathbf{p}_{D^{*}}^*, \Omega_{D^{*}}^*)$ are the momentum and the angle of D^{*} in the cms rest frame of the D^{*0} and D^{*-} mesons. Ω_{π} denotes the angle of π in the rest frame of $Y(4260)$ and $m_{D^{*} \bar{D}^{*}}$ is the $D^{*0} D^{*-}$ invariant mass.

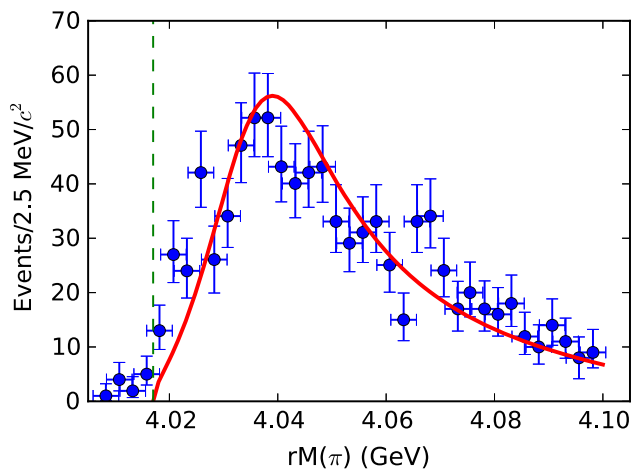


Fig. 4 (Color online) The obtained line shape (red curve) in the $D^* \bar{D}^*$ invariant mass spectrum of $Y(4260) \rightarrow \pi^+ D^{*0} D^{*-}$ and the comparison with the experimental data (blue dots with error) [1]. Here, the green vertical dashed line denotes the $D^* \bar{D}^*$ threshold. Our theoretical result (red curve) is obtained by taking the typical values $g_c = 60.827$, $\phi = 0.986$, and $\xi = 1$

3 Numerical results

With the above analytical calculations, in the following we present the differential decay width of $Y(4260) \rightarrow \pi^+ D^{*0} D^{*-}$ dependent on the $m_{D^* \bar{D}^*}$ invariant mass (see Fig. 4), where three free parameters, g_c , ξ , and ϕ , are involved in our calculation. By this study, we want to answer the question whether the newly observed $Z_c(4025)$ can be reproduced by our model. In our numerical calculation, we only take the $\ell = 0$ partial wave, since its contribution is dominant.

The comparison between our theoretical result and the experimental data indicates that we can simulate the enhancement structure near the $D^* \bar{D}^*$ threshold, which is similar to the $Z_c(4025)$ structure observed by BESIII as just shown in Fig. 4. Here, we notice that there appear experimental data below the threshold, which are due to the adopted experimental method, i.e., BESIII has studied the π^\mp recoil mass spectrum [1]. The above comparison between theoretical and experimental results provides direct evidence that the newly observed $Z_c(4025)$ structure can be well understood in terms of the ISPE mechanism.

4 Summary

In summary, a new charged enhancement $Z_c(4025)$ near the $D^* \bar{D}^*$ threshold has been reported by BESIII. This intriguing experimental observation not only makes the family of the charged charmoniumlike structure become abundant, but also it stimulates our interest in revealing the underlying mechanism behind this novel phenomenon. In this work, we study the $Y(4260) \rightarrow \pi^+ D^{*0} D^{*-}$ decay via the ISPE mech-

anism, where the involved $D^{*0} D^{*-} \rightarrow D^{*0} D^{*-}$ interaction is considered by introducing the ladder diagrams. Our result shows that there exists an enhancement structure near the $D^* \bar{D}^*$ threshold appearing in the $D^* \bar{D}^*$ invariant mass spectrum of $Y(4260) \rightarrow \pi^+ D^{*0} D^{*-}$, which can correspond to the newly observed $Z_c(4025)$. This fact indicates that the ISPE mechanism existing in the $Y(4260)$ decays can be seen as one of the possible mechanisms to explain this new BESIII observation.

At present, experimental work has made great progress in searching for charged bottomoniumlike and charoniumlike structures. Studying these phenomena is an interesting research topic full of challenges and opportunities. Further theoretical and experimental efforts will be helpful to finally understand what the reason is for the phenomena revealed in these observations.

Before closing this section, we need to discuss further developments of our model.

1. In this work, we have neglected the coupled-channel effect arising from one-loop box diagrams like $D^{*0} D^{*-} \rightarrow D^0 D^- / D^{*0} D^- / D^0 D^{*-} \rightarrow D^{*0} D^{*-}$ via two π^0 exchange. Hence, in the next step, we need to include the coupled-channel effect in our model.
2. In this work, we introduce only the imaginary part of the loop when calculating the diagrams listed in Fig. 3. To some extent, this treatment is an approximation. Hence, we need to develop our model to include the real part of the loop diagrams.

Acknowledgments This project is supported by the National Natural Science Foundation of China under Grants No. 11222547, No. 11175073, No. 11005129 and No. 11035006, the Ministry of Education of China (FANEDD under Grant No. 200924, SRFDP under Grant No. 20120211110002, NCET, the Fundamental Research Funds for the Central Universities), the Fok Ying Tung Education Foundation (No. 131006), and the West Doctoral Project of the Chinese Academy of Sciences.

Open Access This article is distributed under the terms of the Creative Commons Attribution License which permits any use, distribution, and reproduction in any medium, provided the original author(s) and the source are credited.

Funded by SCOAP³ / License Version CC BY 4.0.

Appendix A: Relation between partial wave and two-particle bases

A two-particle state, which is characterized by the three-momenta \mathbf{p}_1 , \mathbf{p}_2 and the z -components σ_1 , σ_2 of the corresponding spins s_1 , s_2 , can be defined as $|\mathbf{p}_1, \mathbf{p}_2, s_1, s_2, \sigma_1, \sigma_2\rangle$, which satisfies the normalization

$$\begin{aligned} \langle \mathbf{p}'_1, s'_1, \sigma'_1; \mathbf{p}'_2, s'_2, \sigma'_2 | \mathbf{p}_1, s_1, \sigma_1; \mathbf{p}_2, s_2, \sigma_2 \rangle \\ = \delta^3(\mathbf{p}_1 - \mathbf{p}'_1) \delta^3(\mathbf{p}_2 - \mathbf{p}'_2) \delta_{s'_1 s_1} \delta_{s'_2 s_2} \delta_{\sigma'_1 \sigma_1} \delta_{\sigma'_2 \sigma_2} \end{aligned} \quad (14)$$

with $\tilde{\delta}^3(\mathbf{p}) = (2\pi)^3 2E\delta^3(\mathbf{p})$. The completeness condition gives

$$\sum_{s_1, s_2, \sigma_1, \sigma_2} \int d^3 \tilde{p}_1 d^3 \tilde{p}_2 |\mathbf{p}_1, s_1, \sigma_1; \mathbf{p}_2, s_2, \sigma_2\rangle \times \langle \mathbf{p}_1, s_1, \sigma_1; \mathbf{p}_2, s_2, \sigma_2| = 1, \quad (15)$$

where $d^3 \tilde{p} = d^3 p / ((2\pi)^3 2E_p)$.

A partial wave basis can be expressed in terms of two-particle bases as

$$|p, j, \sigma, \ell, s\rangle = \frac{1}{2(2\pi)^3} \sqrt{\frac{p}{E_p}} \sum_{m, \ell_z} (s_1, \sigma_1; s_2, \sigma_2 | s, m) (s, m; \ell, \ell_z | j, \sigma) \times \int d\Omega_{p_1} Y_{\ell}^{\ell_z}(\Omega_{p_1}) |\mathbf{p}_1, s_1, \sigma_1; \mathbf{p}_2, s_2, \sigma_2\rangle, \quad (16)$$

where Ω_{p_1} is the solid angle of the momentum \mathbf{p}_1 , $Y_{\ell}^{\ell_z}(\Omega_{p_1})$ denotes spherical harmonics, $\vec{j} = \vec{\ell} + \vec{s}$ and $\vec{s} = \vec{s}_1 + \vec{s}_2$. We also define the four-momentum $p = p_1 + p_2$ and E_p is the zeroth component of p . In addition, $(s_1, \sigma_1; s_2, \sigma_2 | s, m)$ and $(s, m; \ell, \ell_z | j, \sigma)$ are the Clebsch–Gordan coefficients. A partial wave basis satisfies the normalization

$$\langle p', j', \sigma', \ell', s' | p, j, \sigma, \ell, s \rangle = \delta^4(p' - p) \delta_{j'j} \delta_{\sigma'\sigma} \delta_{\ell'\ell} \delta_{s's'}. \quad (17)$$

The completeness condition gives

$$\sum_{j, \sigma, \ell, s} \int d^4 p |p, j, \sigma, \ell, s\rangle \langle p, j, \sigma, \ell, s| = 1. \quad (18)$$

The inner product of two different bases is given by

$$\begin{aligned} &\langle \mathbf{p}_1, s_1, \sigma_1; \mathbf{p}_2, s_2, \sigma_2 | p, j, \sigma, \ell, s \rangle \\ &= 2(2\pi^3) \sqrt{\frac{E}{|\mathbf{p}|}} \delta^4(p_1 + p_2 - p) \\ &\times \sum_{m, \ell_z} (s_1, \sigma_1; s_2, \sigma_2 | s, m) (s, m; \ell, \ell_z | j, \sigma) Y_{\ell}^{\ell_z}(\Omega_{p_1}). \end{aligned} \quad (19)$$

Any amplitude can be expressed as a tensor form in terms of partial wave bases,

$$\langle q, \tilde{j}, \tilde{\sigma}, \tilde{\ell}, \tilde{s} | T | p, j, \sigma, \ell, s \rangle = \mathcal{T}^{(j)}(p)_{\ell, s}^{\tilde{\ell}, \tilde{s}} \delta^4(p - q). \quad (20)$$

Here, we need to notice that Eq. (20) is independent on the quantum numbers \tilde{j} , $\tilde{\sigma}$, and \tilde{s} , which is consistent with the constraint from the Wigner–Eckart theorem.

References

1. M. Abilikhim et al. [BESIII Collaboration], [arXiv:1308.2760](#) [hep-ex]. (0000)
2. I. Adachi et al. [Belle Collaboration], [arXiv:1209.6450](#) [hep-ex]. (0000)
3. D.-Y. Chen, X. Liu and T. Matsuki, [arXiv:1208.2411](#) [hep-ph]. (0000)
4. D.-Y. Chen, X. Liu, Phys. Rev. D **84**, 094003 (2011). [arXiv:1106.3798](#) [hep-ph]
5. I. Adachi [Belle Collaboration], [arXiv:1105.4583](#) [hep-ex]. (0000)
6. D.-Y. Chen, X. Liu, Phys. Rev. D **84**, 034032 (2011). [arXiv:1106.5290](#) [hep-ph]
7. D.-Y. Chen, X. Liu, T. Matsuki, Phys. Rev. Lett. **110**, 232001 (2013). [arXiv:1303.6842](#) [hep-ph]
8. D.-Y. Chen, X. Liu and T. Matsuki, [arXiv:1306.2080](#) [hep-ph]. (0000)
9. D.-Y. Chen, X. Liu, T. Matsuki, Phys. Rev. D **84**, 074032 (2011). [arXiv:1108.4458](#) [hep-ph]
10. D.-Y. Chen, X. Liu, T. Matsuki, Eur. Phys. J. C **72**, 2008(2012). [arXiv:1112.3773](#) [hep-ph]
11. E.E. Salpeter, H.A. Bethe, Phys. Rev. **84**, 1232 (1951)
12. Ö. Kaymakçalan, S. Rajeev, J. Schechter, Phys. Rev. D **30**, 594 (1984)
13. Y. S. Oh, T. Song and S. H. Lee, Phys. Rev. C **63**, 034901 (2001). [arXiv:nucl-th/0010064](#)
14. R. Casalbuoni, A. Deandrea, N. Di Bartolomeo, R. Gatto, F. Feruglio, G. Nardulli, Phys. Rept. **281**, 145 (1997). [arXiv:hep-ph/9605342](#)
15. K.L. Haglin, Phys. Rev. D **61**, 031902 (2000)
16. P. Colangelo, F. De Fazio, T.N. Pham, Phys. Lett. B **542**, 71 (2002). [arXiv:hep-ph/0207061](#)
17. S. Ahmed et al. [CLEO Collaboration], Phys. Rev. Lett. **87**, 251801 (2001). [arXiv:hep-ex/0108013](#)
18. C. Isola, M. Ladisa, G. Nardulli, P. Santorelli, Phys. Rev. D **68**, 114001 (2003). [arXiv:hep-ph/0307367](#)
19. G.Y. Chen, J.P. Ma, Phys. Rev. D **83**, 094029 (2011). [arXiv:1101.4071](#) [hep-ph]
20. G.Y. Chen, H.R. Dong, J.P. Ma, Phys. Lett. B **692**, 136 (2010). [arXiv:1004.5174](#) [hep-ph]
21. G.Y. Chen, H.R. Dong, J.P. Ma, Phys. Rev. D **78**, 054022 (2008). [arXiv:0806.4661](#) [hep-ph]